Int J Appl Earth Obs Geoinformation 76 (2019) 26–39

Contents lists available at ScienceDirect

Int J Appl Earth Obs Geoinformation

journal homepage: www.elsevier.com/locate/jag

Identification and mapping of winter wheat by integrating temporal change information and Kullback–Leibler divergence

Xiwang Zhang[a,c,*], Fang Qiu[b], Fen Qin[a]

[a] Key Laboratory of Geospatial Technology for Middle and Lower Yellow River Regions, Ministry of Education, Kaifeng 475004, China
[b] Department of Geospatial Science, University of Texas at Dallas, 800 W Campbell Rd. GR31, Richardson, TX 75080-3021, USA
[c] Institute of Urban Big Data, Henan University, Kaifeng 475004, China

ARTICLE INFO

Keywords:
KL divergence
Temporal change information
Remote sensing
Winter wheat

ABSTRACT

Crop acreage and its spatial distribution are a base for agriculture related works. Current research combining medium and low spatial resolution images focuses on data fusion and unmixing methods. The purpose of the former is to generate synthetic fine spatial resolution data instead of directly solving the problem. In the latter, high-resolution data is only used to provide endmembers and the result is usually an abundance map rather than the true spatial distribution data. To solve this problem, this paper designs a conceptual model which divides the study area into different types of pixels at a MODIS 250 m scale. Only three types of pixels contain winter wheat, i.e., pure winter wheat pixels (P_A), the mixed pixels comprising winter wheat and other vegetation (M_A) and the mixed pixels comprising winter wheat and other crops (M_B). Different strategies are used in processing them. (1) Within the pure cultivated land pixels, the Kullback–Leibler (KL) divergence is employed to analyze the similarity between unknown pixels and the pure winter wheat samples on the temporal change characteristics of NDVI. Further P_A is identified. (2) For M_A, a proposed reverse unmixing method is firstly used to extract the temporal change information of cultivated land components, after which winter wheat is identified from the cultivated land components as previously described. (3) For M_B which only appears on the border of P_A, a mask is created by expanding the P_A and temporal difference is utilized to identify winter wheat under the mask. Finally, these three results are integrated at a TM scale with the aid of 25 m resolution land use data. We applied the proposed solution and obtained a good result in the main agricultural area of the Yiluo River Basin. The identified winter wheat planting acreage is 161,050.00 hm^2. The result is validated based on the five-hundred random validation points. Overall accuracy is 94.80% and Kappa coefficient is 0.85. This demonstrates that the temporal information reflecting crop growth is also an important indicator, and the KL divergence makes it more convenient in identifying winter wheat. This research provided a new perspective for the combination of low and medium spatial resolution remote sensing images. The proposed solution can also be effectively applied in other places and countries for the crop which has a clear temporal change characteristic that is different from others.

1. Introduction

Since China is a large country in terms of its population and agricultural production, a fluctuation of the total yield of Chinese crops will not only affect social stability but also the world agricultural market (Wang et al., 2010; Wu and Li, 2012). In agricultural research, crop acreage and its spatial distribution data constitute a basis for researching the regional balance of food supply, forecasting the comprehensive production capacity of agricultural resources and the population carrying capacity (Lobell et al., 2015; Waldhoff et al., 2017). Winter wheat is one of the most important food crops in the world, and the largest share of global production is concentrated in China, contributing to 17.3% of global production (Franch et al., 2015; Ren et al., 2008; FAOSTAT, 2014). Quickly and accurately acquiring winter wheat acreage and distribution in China is very important and also a challenge due to the small field sizes and particular management practices (Yang et al., 2017; Liaghat and Balasundram, 2010).

Remote sensing has proven to be an effective tool and been widely used in the agricultural field (Wu et al., 2017; Qiu et al., 2017; Li et al., 2017). It can help acquire large-area data recurrently (Wu et al., 2017; Homolova et al., 2013), and can monitor agricultural production changes and the resource utilization status in order to help quickly grasp agricultural information and assist macro-control (Hao et al., 2015). Quickly and accurately obtaining crop information based on

* Corresponding author.
E-mail address: zxiwang@163.com (X. Zhang).

https://doi.org/10.1016/j.jag.2018.11.002
Received 12 August 2018; Received in revised form 5 November 2018; Accepted 6 November 2018
Available online 16 November 2018
0303-2434/

remote sensing is a key technical problem (Waldner et al., 2015). Usually, winter wheat can be classified based on spectral characteristics using remote sensing technology because different land cover types have different spectral curves (Yusoff and Muharam, 2015; Everitt et al., 2013; Landmann et al., 2015). In an ideal period of crop growth, high (< 10 m) or medium (10–100 m) spatial resolution remote sensing images can help to monitor relatively accurate planting acreage (Pax-Lenney et al., 2001; Martínez-Casasnovas et al., 2005). However, ideal optical remote sensing images may not be obtained during a specific period due to factors such as weather conditions or the revisit cycle (Conese and Maselli, 1991; Castillejo-González et al., 2009; Whitcraft et al., 2015; Wu et al., 2016a; Wang et al., 2017). Temporal characteristics are also a widely used feature for crop mapping (Li et al., 2014; Siachalou et al., 2015; Jin et al., 2016). Time series image data, such as NOAA/AVHRR (1.1 km), SPOT/VEGETATION (1.15 km), and TERRA/MODIS (250 m–1000 m), can characterize crop phenology and are used to identify crop types based on temporal change information (Qin et al., 2015; Upadhyay et al., 2015). Pan et al. (2012) proposed a Crop Proportion Phenology Index (CPPI) following the concept of a Vegetation Index using the peaks and troughs of EVI time series curve to assess the quantitative relationship between the MODIS vegetation index time series and winter wheat crop area. Gumma et al. (2015) used MODIS 250 m 8-day time series data to map the spatial distribution of rice areas based on spectral matching techniques. Sun et al. (2012) developed a curve-shaped based method to map winter wheat planting area based on time series MODIS vegetation index data. Essentially, this kind of time-series based approaches all rely on the similarities with the temporal profile of standard vegetation indices from other vegetation or crop types. As the variant of these methods, some phenological metrics based approaches are developed. They assess vegetation similarity based on specific components or statistical characteristics of a time series (Lhermitte et al., 2011; Wardlow and Egbert, 2010; Gao et al., 2017). However, the spatial resolution of these data is usually low and does not provide sufficient details on spatial change characteristics; thus, the positional accuracy is low, especially in complex planting areas (Zheng et al., 2012; Estel et al., 2015). Therefore, spectral information from high- or medium-resolution remote sensing and temporal information from low-resolution remote sensing are usually used in combination (Langley et al., 2001; Lobell and Asner, 2004; Wu et al., 2015).

In applications combining spectral and temporal features, some researchers have proposed data fusion approaches to combine spectral and temporal information, improving crop mapping accuracy (van Lier et al., 2009; Wu et al., 2016b). Wu et al. (2016b) introduced an improved spatial and temporal data fusion approach (ISTDFA) to generate daily synthetic Landsat imagery by combining Landsat and MODIS data. Zhu et al. (2016) presented a Flexible Spatiotemporal Data Fusion (FSDAF) method to generate synthesized frequent high spatial resolution images through blending MODIS and Landsat. It can be seen that these methods are mainly used to generate synthetic fine spatial resolution data rather than to solve practical problems (Wu et al., 2015). Although these fusion methods can facilitate research for specific applications, they face challenges due to their assumptions and harsh input data and usually also do not work well in complex heterogeneous or frequently disturbed areas (van Lier et al., 2009; Zhu et al., 2016; Amorós-López et al., 2013). Some researchers have focused on the unmixing method of low spatial resolution remote sensing data, in which high-resolution data is only used to provide an endmember (Busetto et al., 2008; Atzberger and Rembold, 2013; Vorobiova and Chernov, 2017). Busetto et al. (2008) proposed an unmixing approach for the sub-pixel abundance estimation using multi-temporal MODIS NDVI data by a weighted linear system taking into account both the spatial distance between each pixel and the target and their spectral dissimilarity, and Landsata 5 TM images were used to provide pure endmember. Atzberger and Rembold (2013) exploited neural networks to learn the relation between temporal AVHRR NDVI signatures and the crop acreage information, and perform a non-linear unmixing of the temporal information provided by coarse resolution images. The reference crop acreage derived from Landsat TM. Potapov et al. (2008) assessed forest cover change by building regression models between low-resolution vegetation index series and identification results of high-resolution remote sensing. This method is essentially exploring the internal information of each pixel, similar to the unmixing approach (Qin et al., 2015). The acreage accuracy of these methods is usually around 90% (Qiu et al., 2017; Tao et al., 2017). However, the results of these methods are the coarse resolution abundance (crop acreage percentage in each pixel), which can be used to calculate acreage but cannot account for the spatial distribution of pixel components (Verhoeye and De Wulf, 2002; Kasetkasem et al., 2005). To solve the problem of component distribution, some sub-pixels mapping solutions have been reported, including two categories: the knowledge-based and spatial dependence based methods (Atkinson, 1997; Tatem et al., 2001; Mertens et al., 2004). The relevant research shows that accuracy can greatly exceed 90% under ideal conditions and that it can decline under real circumstances (Zhong et al., 2014). Among these kinds of methods, the former depends on an accurate boundary that splits the mixed pixels into pure components at a fine spatial resolution (Verhoeye and De Wulf, 2002; Mertens et al., 2003). Tatem et al. (2002) applied a hopfield neural network technique to sub-pixel mapping of land cover, firstly used soft classification to determine information of pixel composition, then the neural network converges to a minimum of an energy function which need a prior boundary information as a constraint. However, the boundary may not be readily available. The latter considers that objects that are close together are more alike than objects that are further apart (Kasetkasem et al., 2005; Thornton et al., 2006). Currently, most sub-pixel mapping techniques are based on this assumption to obtain the spatial distribution of each component by dividing pixels into smaller sub-pixels at a certain scale (Zhong et al., 2014). Simultaneously, they are also based on single images and there is often uncertainty due to insufficient constraint of sub-pixel patterns within the low resolution pixels. In addition, this spatial dependence assumption will cause a more homogenous super-resolution map and the loss of some small targets of interest (Zhong et al., 2014; Wetherley et al., 2017).

Although the aforementioned methods based on unmixing and temporal characteristics have been successfully applied and have achieved very good acreage accuracy (Qiu et al., 2017; Tao et al., 2017), the results are at a coarse resolution scale. To overcome the problems of sub-pixel mapping methods, most researchers usually explore more complex algorithms which are difficult to implement in practice (Huang et al., 2016; Wang and Atkinson, 2017). Little research has paid attention to the combination of these two types of approaches. We integrated their advantages to propose a new solution which is based on time series data rather than single images, thereby eliminating uncertainty to some extent. In our solution, the Kullback–Leibler divergence (KL divergence) is introduced to assess the similarity between the unknown pixel time series and a reference for both pure pixels and sub-pixels. This is a non-parametric approach that does not require the normality of the probability distribution and is widely used in speech, image pattern recognition and hyperspectral image classification (Zhou and Qiu, 2015; Ghiyamat et al., 2013). Another innovation is to propose an unmixing method in which the difference to the traditional methods lies in reverse processing. Additionally, this is used to extract time series information from sub-pixels. In the problem-solving framework, we proposed a conceptual model that divided the study area into different types of pixels at a 250 m scale. Then, different strategies were used for different types of pixels. The aim of this paper is to obtain good results by making more use of data that is easily available, such as land use data and MODIS, and to minimize the use of fine resolution remote sensing images to promote our method within a larger area. The proposed method was implemented in a major agricultural area of the Yiluo River Basin and achieved a good result.

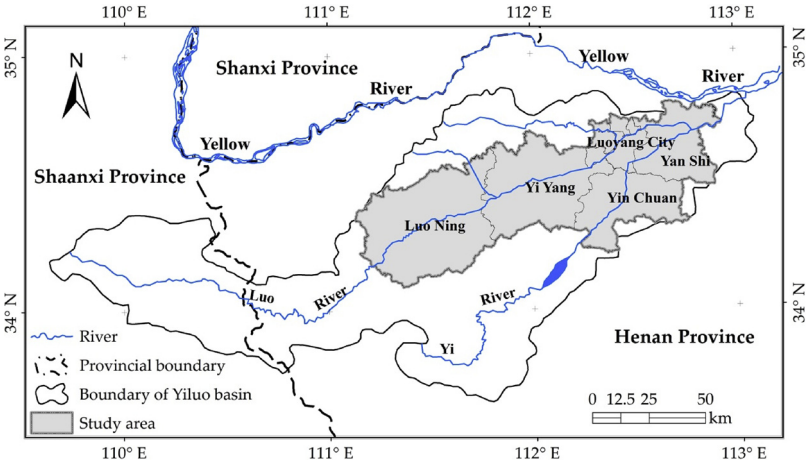

Fig. 1. The study area which is located in the Yiluo River Basin, China.

2. Study area

Wheat is one of the most important food crops in the world, and the largest global production is concentrated in China, contributing to 17.3% of global production, while the production of Henan Province accounts for a quarter of China's production (FAOSTAT, 2014; Zhou et al., 2017). As a typical area, the major agricultural area of the Yiluo River Basin is selected as the study area in this paper. It covers all types of cultivated land and most of the cultivated area of the Yiluo River Basin and includes 5 parts: Luoning, Yiyang, Yichuan, and Yanshi counties, as well as Luoyang city. The total area is approximately 6453.22 km^2, and its geographic coordinates are 34°05′–34°50′ N, 111°06′–112°58′ E (Fig. 1). The Yiluo River is an important tributary of the Yellow River, and it is comprised of the Yi River and Luo River, with a total length of approximately 447 km.

The area is characterized by a continental monsoon climate. The average annual precipitation is approximately 660 mm, and the rainy season accounts for 60% of the annual precipitation and occurs between June and September (Zhang et al., 2013). The main landforms of the study area, mountain and hills, account respectively for 50.7% and 39.9% of the acreage. And the rest is plain, 9.4%. The elevation of the basin gradually decreases from 3100 m to 101 m above sea level from the southwest to the northeast. There are predominantly cinnamon and brown soils whose parent material both are redeposited loess (NSPRC, 2009). Their clay content exceeds 25% and fine sand content is less than 15%, that is conductive to agricultural production. There is also a small amount of red clay soil and purplish soil. Deciduous forests of the warm temperate zone dominate the natural plant communities in this region. The tree species includes *Fagaceae*, *Betulaceae*, *Salicaceae*, *Juglandaceae*, *Aceraceae*, etc.

In the study area, forest, shrub and grass account respectively for 8.1%, 12.1% and 13.7% of the acreage. Water, including river and reservoir, accounts for only 0.8%. Habitant land, traffic and mines together account for about 15.0%. Unused land is rarely, almost negligible. The rest is cultivated land. Winter wheat is the main wintering crop in this study area. Its growth cycle starts in mid-October and ends in mid-June of the second year, passing through the sowing, emergence, tillering, wintering, turning green, jointing, heading, milking and mature stages. A large concentrated planting area occurs in the central and eastern basins.

3. Materials and methodology

In this section, a conceptual model (Fig. 2) is first proposed to divide the study area into different types of pixels at 250 m scale. Only three types of pixels comprise winter wheat. Different strategies are designed to extract winter wheat from them. The flowchart (Fig. 3) shows the detailed process steps.

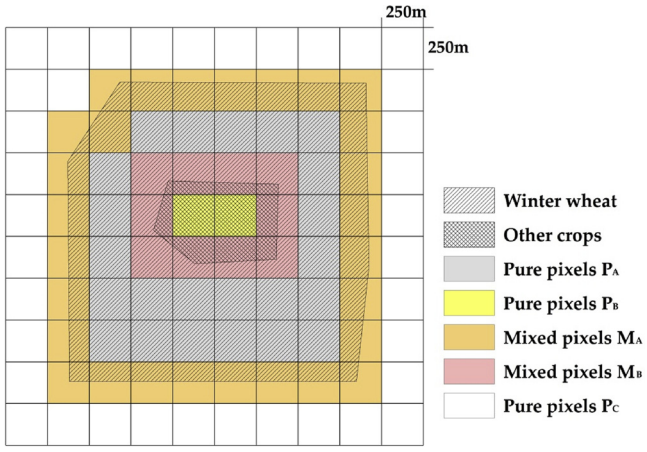

Fig. 2. A conceptual model: the study area is covered by 250 m grid, generating different types of pixels. P_A is a pure pixel entirely composed of winter wheat, P_B is a pure pixel entirely composed of other crops, P_C is a pure pixel entirely composed of other vegetation, M_A is a mixed pixel composed of winter wheat (or other crops) and other vegetation, and M_B is a pixel composed of winter wheat and other crops.

3.1. Conceptual model and workflow

3.1.1. Design of conceptual model

The study area can be generalized as shown in Fig. 2. The part covered by a slash is the winter wheat planting area, while the parts covered by the slash grid are the planting areas of other crops; the blank part is non-cultivated land. If the study area is overlaid by a square grid layer with a 250 m resolution, similar to a MODIS image, five types of pixels will be generated, as follows: (1) pure pixels completely formed by winter wheat, that is P_A; (2) pure pixels completely formed by other crops, P_B; (3) mixed pixels constituted by other vegetation and winter wheat, or by other crops, M_A; (4) mixed pixels consisting of winter wheat and other crops, M_B; and (5) pure pixels completely formed by other vegetation, P_C.

From Fig. 2, it can be seen that winter wheat may only appear in P_A, M_A and M_B. In addition, cultivated land is composed of P_A, P_B, M_A and M_B. Conversely, if the cultivated land is known in the study area, its pure pixels contain P_A, P_B and M_B, and its mixed pixels are M_A. Therefore, only three types of pixels (P_A, M_A and M_B) need to be addressed for the winter wheat acreage estimation. Based on the

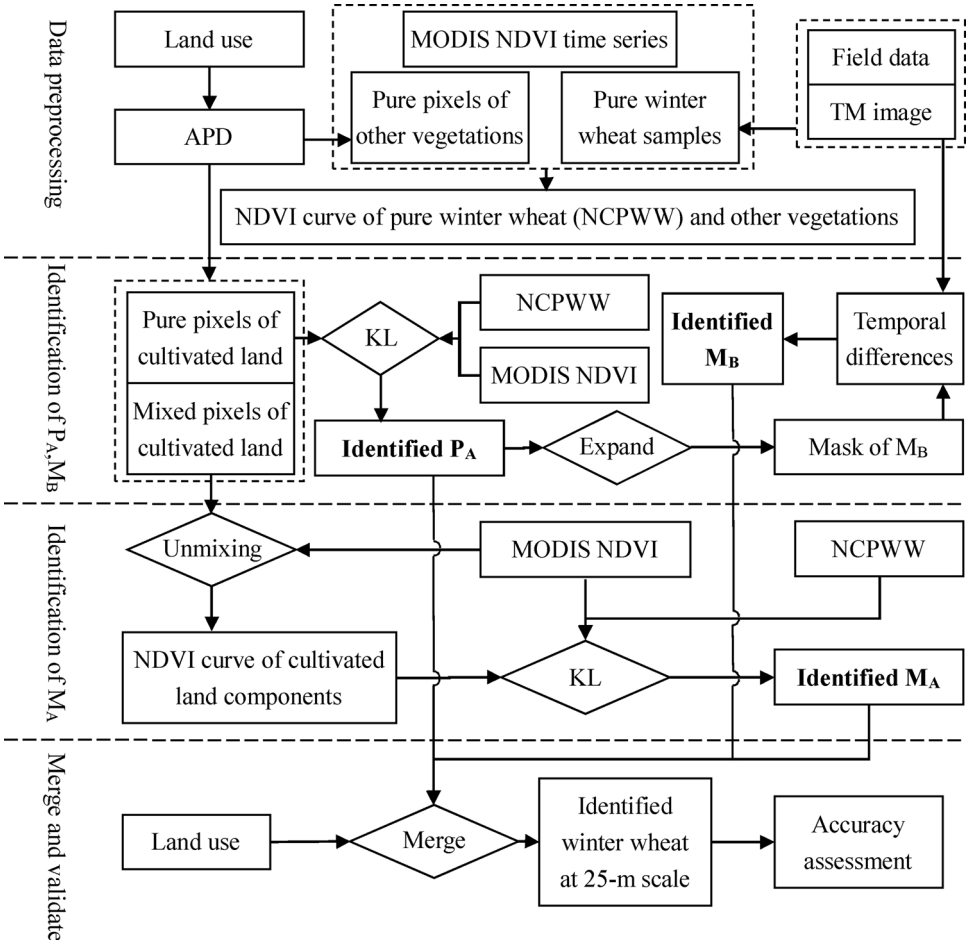

Fig. 3. Flowchart of winter wheat identification in this study. KL means Kullback–Leibler divergence, APD means Acreage Percentage Data and S-G means Savitzky-Golay filter.

aforementioned analysis, we will identify winter wheat by processing the different types of pixels using different strategies.

3.1.2. Workflow for winter wheat identification

The steps for identifying winter wheat are summarized in Fig. 3.

Based on the conceptual model, it involves 4 major processes to identify winter wheat. The KL divergence is used in the process of identifying P_A and M_A. And the proposed mixed pixel unmixing method is utilized in identifying M_A. The detailed steps are as follows:

(1) Landsat TM image is used to obtain the reference pure winter wheat samples based on field survey experience. Land use data is used to generate acreage percentage data (APD), in which pure pixels from other land use types can be acquired. Then, time series curves of winter wheat and other land use types can be extracted from MODIS time series data.
(2) The KL divergence is employed to assess the similarity of unknown pixels and reference winter wheat in temporal change information to get pure winter wheat P_A. A mask is obtained by expanding the identified P_A. The M_B containing winter wheat is identified under the mask based on the temporal difference.
(3) Using the proposed unmixing method, a NDVI curve of cultivated land components in mixed pixels is extracted from the MODIS time series data. The KL divergence is also utilized to identify winter wheat at a sub-pixel scale.
(4) Finally, the three results are integrated with the aid of land use data at a 25 m scale.

3.2. Datasets and processing method

3.2.1. Data collection

Three types of data were collected in identifying winter wheat in this research. NDVI time series was used to characterize the process of vegetation growth and identify winter wheat from temporal characteristics. Landsat TM was utilized to correct the land use data and also used to assist the validation of the result. Land use data was exploited to provide the components of each land use type, and also used to assist in sample selection and generating NDVI time series curves. To validate the result, official statistics data and field data was also collected.

3.2.1.1. NDVI time series. The NDVI (Normalized Difference Vegetation Index) has been widely used in vegetation studies (Aguilar et al., 2012). As the best indication factor of vegetation dynamics and spatial distribution, it is a linear correlation with vegetation distribution density (Gandhi et al., 2015). NSAS Earthdata website (http://reverb.echo.nasa.gov/) offers three resolutions of vegetation index products, 1000 m, 500 m and 250 m. Based on the size of study area, MOD13Q1 and MYD13Q1 with a 250 m spatial resolution were downloaded for free and selected in this research. Even in a period that is frequently cloud-covered, there is the opportunity to acquire cloudless images or synthetic products of a very high frequency. Both these two datasets are 16-day synthesis data respectively from Terra and Aqua. There is an 8-day interval in time, so they are combined to form an eight-day NDVI time series in this paper.

3.2.1.2. Landsat TM. In this study, we used a geometrically and

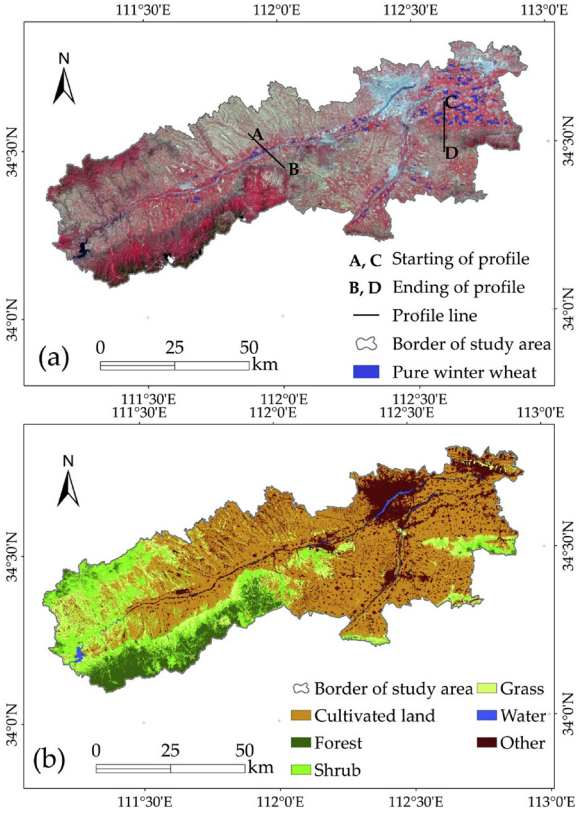

Fig. 4. (**a**) Landsat-5 T M image after being resampled using a 25 m resolution, which is covered by a scene (path 125 and row 36) acquired on May 2, 2010 (RGB = Bands4,3,2). The blue polygons are pure winter wheat samples which are created using 250 m grid corresponding to MODIS data. And the two black lines are spatial profile lines. (b) Land use data of the study area which is rasterized at a resolution of 25 m (For interpretation of the references to colour in this figure legend, the reader is referred to the web version of this article).

radiometrically corrected Landsat TM image acquired on May 2, 2010, with a 30 m spatial resolution. It is the only cloudless Landsat image of high quality during the winter wheat growing season covering the entire study area, as shown in Fig. 4a. It is necessary to spatially match the MODIS data at pixel scale in our proposed method, so the Landsat TM image is resampled using a 25 m resolution. After the spatial registration with MODIS data, each 250 m MODIS pixel will correspond to 10 × 10 TM pixels.

3.2.1.3. Land use. The land use dataset of 2010 was a vector map and downloaded from the national earth system science data sharing infrastructure, China (http://www.geodata.cn/). It was extracted from Landsat TM images and calibrated based on field data. Before using this data, we further calibrated the data in the study area. With the aid of the field data, the land use data is corrected by visual interpretation based on Landsat TM images. The overall accuracy is guaranteed to be over 98.5%. According to the characteristics of vegetation cover types, land use data were merged into six categories: forest, shrub, grass, cultivated land, water and other. The data were also rasterized at a resolution of 25 m due to the same reason as above, as shown in Fig. 4b.

3.2.1.4. Official statistics data. Crop acreage data were collected from the statistics department of Henan province in China. Among them, the 2011 official statistics record the winter wheat planting acreage of 2010. These data will be compared to the results of this study in order to verify the effectiveness of the proposed method.

3.2.1.5. Field work and validation data. Field work was carried out in May 2010 to investigate land use and vegetation types, with locations recorded by GNSS equipment with an estimated positional accuracy of ± 15 m. These field data were primarily used to assist the remote sensing interpretation and correct the land use dataset.

Five-hundred validation points in the study area were generated randomly using GIS software. Combined with field data and interpretation experience, each point was visually interpreted at the location based on the TM image. The interpreted points were used to validate the winter wheat identification results of this study.

3.2.2. Data preprocessing

3.2.2.1. Producing acreage percentage data (APD). In this paper, acreage percentage data (APD) refers to the acreage ratio of land use types in a pixel. And its pixel value range is [0, 1]. Based on GIS technology, the corrected land use data based on Landsat TM images are used to produce APD with a 250 m resolution. Each APD pixel value can be obtained from the statistics of its corresponding 10 × 10 25 m land use pixels. Then, APD will be used to extract pure pixels of land cover types. It will also be used as an input parameter for the unmixing model in this research.

In the study area, a water body only includes rivers and reservoirs. Its spectral characteristics are distinctly different from other objects and are considered as a separate category in this paper. The NDVI value of a water body is very small, but it also changes with time due to the influence of aquatic vegetation and other factors.

Habitant land, traffic, mines and unused land are integrated as an "other" type. The features of its NDVI time series mainly reflect the changes of internal green vegetation.

3.2.2.2. Processing and analysis of NDVI time series. For winter wheat, pure samples were selected from TM images using 250 m grid corresponding to MODIS data based on visual interpretation. The selected samples should be in homogeneous planting areas, avoiding other small objects, to ensure that they really are pure winter wheat pixels. In this research, 93 winter wheat samples were selected for a total of 82.62 km^2, as can be seen in Fig. 4a. For other land use types, the pixels with a value of 1 are selected as pure samples in the APD. Following this, the samples were used to extract their respective NDVI curves from the MODIS NDVI time series. The extracted time series data were processed using the Savitzky-Golay filtering method to eliminate jagged irregular fluctuations of the curve (Jönsson and Eklundh, 2004; Chen et al., 2004).

After the pure pixels time series curves are processed by the Savitzky-Golay filter, it is shown in Fig. 8. For winter wheat, the distinctive feature points differing from the other land use types can be found from this Figure. Point A is the beginning of the entire growing season. The first peak forms at point B due to the start of the wintering stage. During the period AB, NDVI of winter wheat increases, whereas the NDVI values of the others gradually decline, forming a great contrast. From point C in the second year, winter wheat begins to wake up and grows rapidly until point D, whereas the others have not yet begun to grow and their NDVI values have not significantly increased. Therefore, there is a significant difference in the changes of NDVI value during the period CD. Winter wheat begins to mature at point E, after which its leaves begin to yellow and the NDVI begins to decrease, thus forming the second peak E, whereas the others continue to grow. Point F corresponds to harvest time. During the period EF, the NDVI of winter wheat rapidly declines, whereas the others do not possess this characteristic.

Therefore, the winter wheat NDVI time series curve can be characterized by the six key feature points (A, B, C, D, E and F). The data at the key feature points are selected to analyze the difference from other land use types. The appearance times of the key features are not necessarily identical because of the impact of weather, planting habits, terrain, etc. To improve stability, the data of the key feature points are processed as follows:

$$NDVI_X = Average \quad (NDVI_{X-1}, NDVI_X, NDVI_{X+1}) \tag{1}$$

where $NDVI_X$, $NDVI_{X-1}$ and $NDVI_{X+1}$ are, respectively, the corresponding NDVI value of point X, and the points before and after X in the time series; X is one of the points A, B, C, D, E or F.

3.3. Kullback–Leibler (KL) divergence

In probability and information theories, the KL divergence is a measure of the difference between two probability distributions P and Q (Kullback and Leibler, 1951). For discrete probability distributions P and Q, the KL divergence from Q to P is defined (Zhou and Qiu, 2015; Olszewski, 2012) as shown in Eq. (2):

$$D_{KL}(P||Q) = \sum_{i}^{n} P(i)\log\frac{P(i)}{Q(i)} \tag{2}$$

where P typically represents the "true" distribution of data, while Q typically represents an approximation of P. In this paper, P refers to the probability distribution of the NDVI time series data of a reference pure winter wheat NDVI curve, while Q refers to that of an unidentified pixel; i refers to the ith NDVI value in a time series, and n refers to the number of the time series data.

Although the KL divergence is often intuited as a means of measuring the distance between probability distributions, it is not symmetric, i.e., $D_{KL}(P||Q) \neq D_{KL}(Q||P)$. The mutual KL divergence $\bar{D}$ between P and Q is symmetric and nonnegative and is calculated as Eq. (3):

$$\bar{D} = (D_{KL}(P||Q) + D_{KL}(Q||P))/2 \tag{3}$$

$\bar{D}$ is the dissimilarity measurement between the time series curve of an unknown pixel and a reference curve.

3.4. Mixed pixel unmixing method

Inevitably, because of the low spatial resolution of the MODIS data, there are mixed pixels. In this paper, we proposed a pixel unmixing method in order to extract the NDVI time series information of a component from the MODIS data. This is an opposite process to a normal pixel unmixing method, which is used to extract acreage percentage.

Assuming that there are three components, X, Y and Z in a MODIS pixel (Fig. 5) and that their contributions are I_X, I_Y and I_Z, respectively, the overall information I can be expressed as Eq. (4):

$$I = I_X + I_Y + I_Z \tag{4}$$

If the acreage ratios of the three components in the MODIS pixel are, respectively, α, β and γ, and the pure pixel information is, respectively, I_x, I_y and I_z, Eq. (4) can be rewritten as Eq. (5):

$$I = I_x\cdot\alpha + I_y\cdot\beta + I_z\cdot\gamma \tag{5}$$

In this Equation, $I_x\cdot\alpha$, $I_y\cdot\beta$, and $I_z\cdot\gamma$ represent the components' contributions to the MODIS pixel information. If the information refers to NDVI, then Equation (5) can be expressed as Eq. (6):

$$NDVI = NDVI_x\cdot\alpha + NDVI_y\cdot\beta + NDVI_z\cdot\gamma \tag{6}$$

Assuming there is a certain proportion for the NDVI information of the three components at a certain time when the pixel unmixing is required, that is, as shown in Eq. (7):

$$NDVI_x : NDVI_y : NDVI_z = k : m : l \tag{7}$$

Then, combining Eqs. (6) and (7), the NDVI information of each component can be calculated as Eq. (8):

$$\begin{cases} NDVI_x = \frac{k\cdot NDVI}{k\cdot\alpha + m\cdot\beta + l\cdot\gamma} \\ NDVI_y = \frac{m\cdot NDVI}{k\cdot\alpha + m\cdot\beta + l\cdot\gamma} \\ NDVI_z = \frac{l\cdot NDVI}{k\cdot\alpha + m\cdot\beta + l\cdot\gamma} \end{cases} \tag{8}$$

where $NDVI$ is the NDVI value of the MODIS pixel and is known; α, β and γ are the acreage percentage of components in the MODIS pixel and can be obtained from Fig. 7; and $NDVI_x$, $NDVI_y$ and $NDVI_z$ are the NDVI values of the pure pixels of the three components. Zhang (2009) has proven that k: m: l can be represented by the ratio of NDVI means of the pure pixels of the three components at the same time (Zhang, 2009). Therefore, Eq. (8) is solvable.

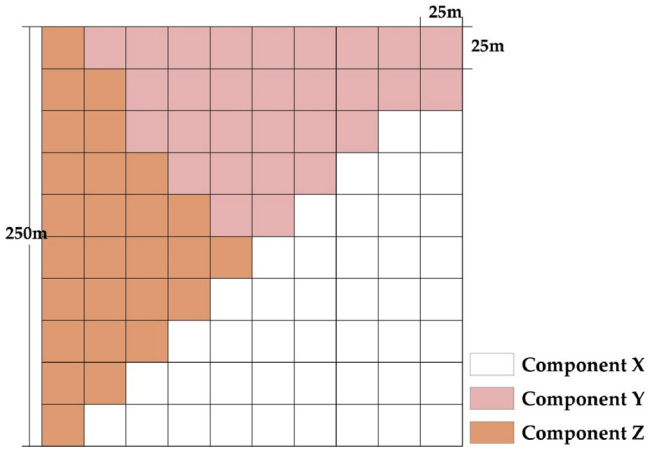

Fig. 5. Schematic diagram of MODIS mixed pixels with three components. A MODIS pixel corresponds to 10 × 10 25 m TM pixels.

3.5. Extraction of winter wheat

3.5.1. Identification of P_A

Many researchers have demonstrated that each type of vegetation, including crops, has unique temporal change features that are different from other vegetation types (Qin et al., 2015; Chmielewski et al., 2004; Sakamoto et al., 2005). These features are codetermined by environmental conditions and agronomic practices (He et al., 2015), and they are an important foundation for distinguishing crop types (Qin et al., 2015). Fig. 8 shows that the temporal variation of winter wheat is obviously different from other vegetation. We made decisions on unknown pixels according to their similarity with the NDVI time series of pure winter wheat samples.

The KL divergence was originally introduced as a dissimilarity measurement between two probability distributions, before being used in the classification of images based on changes in the spectral domain, and it obtained good results (Zhou and Qiu, 2015; Xu et al., 2016). In this study, it will be used in the temporal domain in order to identify winter wheat based on changes in NDVI over time. First, the reference time series data is extracted (Fig. 8) and considered as the "true" distribution of data. Then, the divergence values are calculated between the NDVI series of unknown pixels and the reference. Finally, we explore the threshold of pure winter wheat by GIS overlay analysis between pure winter wheat samples and KL divergence data. Expert experience in image interpretation is used to determine whether samples are sufficient. A threshold will be used to extract pure winter wheat pixels at a MODIS scale.

According to the analysis of Section 3.1, pure cultivated land contains pure pixels of winter wheat P_A, pure pixels of other crops P_B and mixed pixels of different crops M_B. Therefore, the remaining pure cultivated land pixels, after identifying P_A, are P_B and M_B. If all crops need to be identified, it is necessary to extract the reference NDVI time series data of each crop. Following this, we can use the aforementioned method to identify the pure pixels of each crop, with the remaining being M_B. This will be our direction for future research.

3.5.2. Identification of M_A

After being strictly registered in space, a MODIS pixel with a 250 m spatial resolution will correspond to 100 land use pixels with a 25 m resolution. For the mixed pixels from cultivated land and non-cultivated land, the pixel unmixing method of Section 3.4 is exploited to extract the NDVI temporal change information of land use components from the MODIS NDVI time series data. After this, the similarity between the NDVI time series of the land use component and the reference data based on the KL divergence is used to make a decision according to Section 3.5.1. If the NDVI time series of the land use component of a mixed MODIS pixel is judged to be equal to the reference data, the land use component part is considered to be covered with winter wheat. By combining the land use data, the identification results can be converted to a 25 m scale according to the spatial relationship between the two datasets.

3.5.3. Identification of M_B

The mixed pixels from different crops are represented by M_B in Fig. 2 and can be obtained from pure cultivated land pixels by removing P_A and P_B. However, the purpose of this study is only to assess winter wheat, and P_B is therefore not specifically processed. In this study, we adopted a simple approach to create M_B. Theoretically, M_B only appears at the borders between winter wheat and other crops. If the boundaries are regular, then M_B will appear only within one pixel near the boundary (e.g. Fig. 6a). If the boundary is very irregular, M_B may appear within more than one pixel (e.g. Fig. 6b). However, very irregular boundaries rarely appear; thus, P_A is expanded by 3 pixels to create a region that can be considered to be M_B. Actually, this region will be slightly larger than M_B because winter wheat dominates the entire study area during this growing season. Winter wheat will be extracted based on temporal differences in the M_B region that is considered as a mask.

3.5.4. Merging the above three identified results

For Section 3.5.1, the identified results are pure winter wheat pixels at a MODIS 250 m scale and can be directly converted to a 25 m scale. For Section 3.5.2, the identified results are also at a MODIS 250 m scale. However, only the cultivated land covered by the identified MODIS pixels is winter wheat. In combination with the cultivated land at a 25 m resolution, this result can also be converted to a 25 m scale. For Section 3.5.3, the identified result is itself at a 25 m scale because it is extracted based on temporal information and land use data. The final identified winter wheat at a 25 m resolution can be obtained by merging the aforementioned three results.

3.6. Validation of results

The randomly generated validation points are used to create confusion matrix. The identification results of the winter wheat planting area are estimated using overall accuracy (OA), producer's accuracy (PA), User's accuracy (UA) and kappa coefficient (Kappa).

4. Results

The input data of the proposed solution, APD and pure pixel NDVI time series, were produced in the data preprocessing. Then, three types of pixels comprising winter wheat was identified by different processing methods. Finally, the winter wheat spatial distribution data with 25 m resolution was achieved by combining the land use data. The detailed results are as follows.

4.1. Acreage percentage data and NDVI time series

4.1.1. Acreage percentage data

In this paper, land use data is merged into six land use types: forest, shrub, grass, cultivated land, water and other. Therefore, the APD image of each type is produced based on GIS technology and shown in Fig. 7. For APD, the pixel value means the acreage ratio of a particular land use type within a pixel, and the value 1 represents a pure pixel.

4.1.2. NDVI time series of pure pixels

By using the pure pixel samples of each land use type, their NDVI time series can be extracted from MODIS data. Then, they are processed by the Savitzky-Golay filter and the corresponding curves are shown in Fig. 8. The curve characteristics of winter wheat are different from others, such as the rapid increase during segment AB, the peaks at B and E, the slope of segment CD and the rapid decrease of segment EF. Thus, six key feature points – A, B, C, D, E, and F – are highlighted. During the growing season, the corresponding actual time of points A, B, C, D, and E are, respectively, November 1, 2009; December 27, 2009; January 25, 2010; March 22, 2010; April 23, 2010; and June 10, 2010. The equivalent stages are seedling, wintering, greening, booting, heading and harvest.

4.2. Pure winter wheat pixels P_A

Pure winter wheat pixels P_A were identified from pure cultivated land pixels based on the KL divergence and the explored threshold (0.0166) at a MODIS scale. This means that the pixel is winter wheat when its KL divergence is less than 0.0166. This is to say that the 100 corresponding pixels at a 25 m resolution each are all winter wheat. The identification results during the 2009–2010 growing season are shown

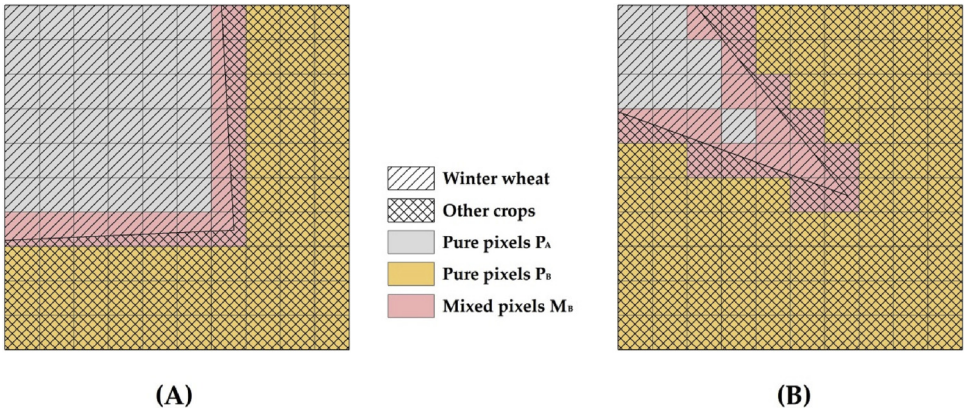

Fig. 6. The relationship between pure pixels P_A and mixed pixels M_B. (A) M_B is generated by expanding P_A by one pixel, (B) In some part, M_B is generated by expanding P_A by three pixels.

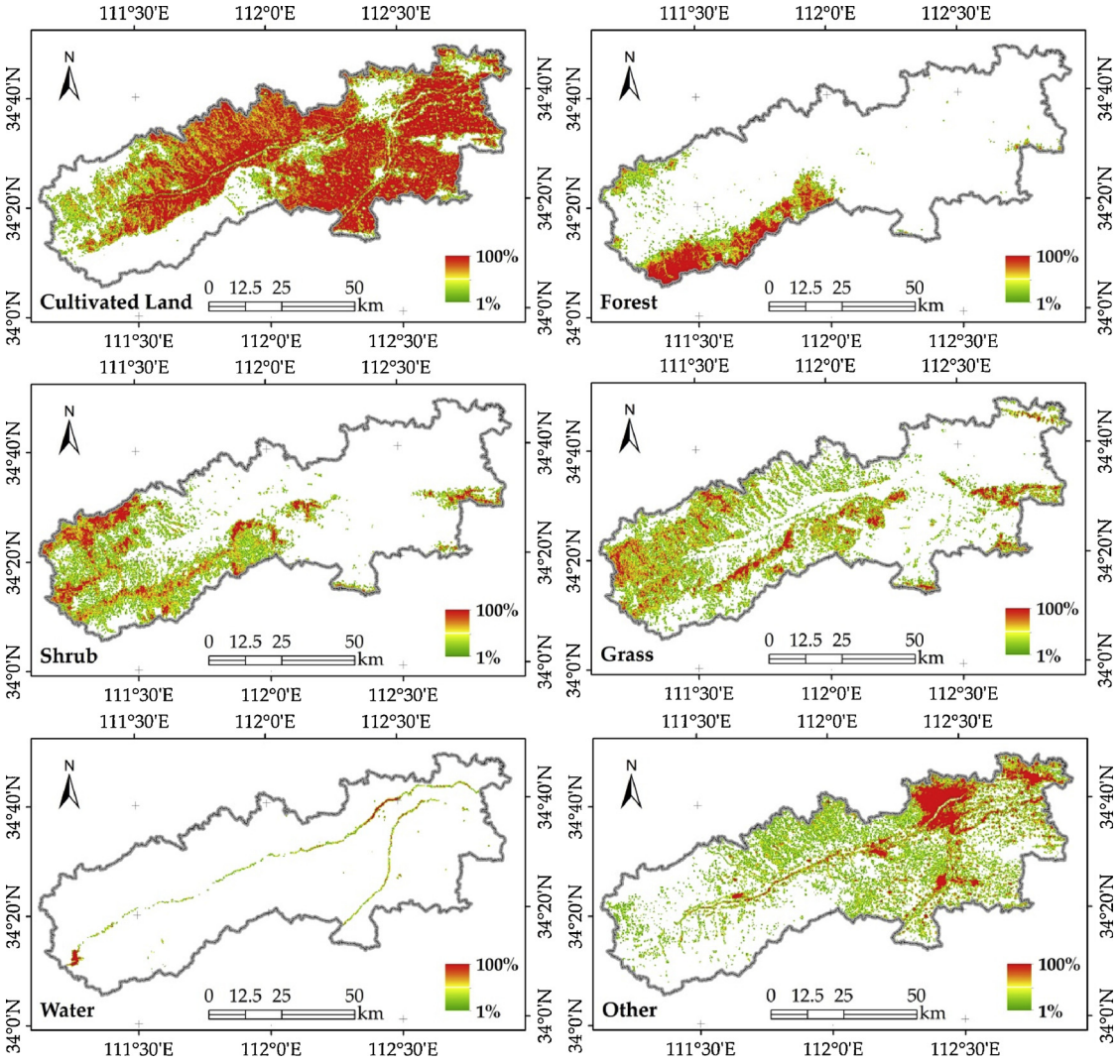

Fig. 7. The acreage percentage data (APD) with 250 m resolution, in which each pixel is formed by aggregating 10 × 10 25 m land use pixels based on GIS technology. For APD of each land use type, the pixel value indicates its acreage ratio within this pixel.

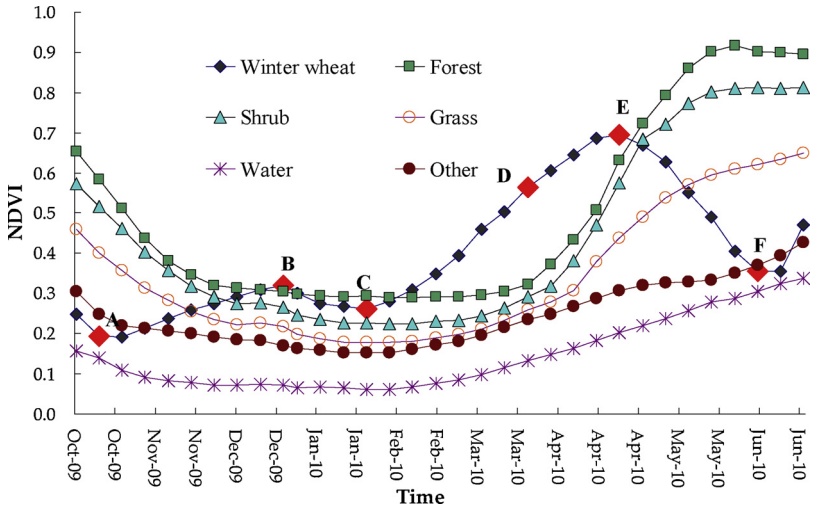

Fig. 8. The pure pixels NDVI time series curves after processing using the Savitzky-Golay filter in the study area. A–F are the key feature points in the time series curve of winter wheat.

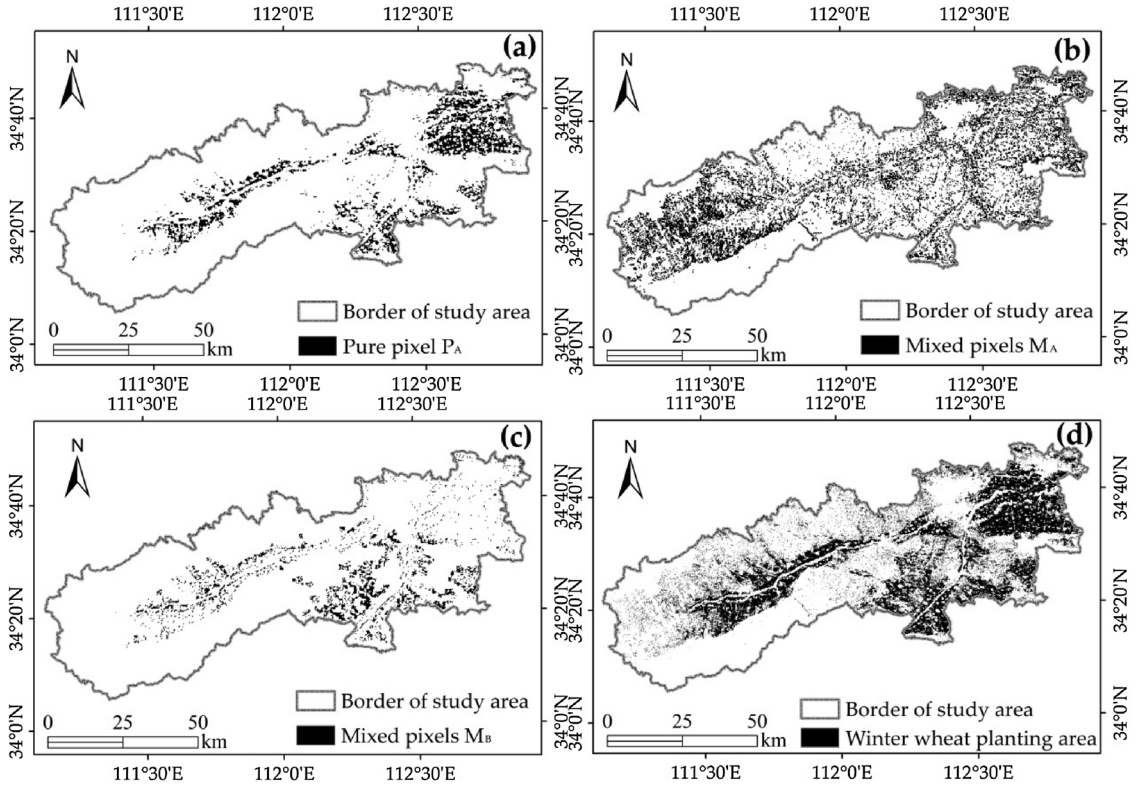

Fig. 9. Extracted results of various pixels containing winter wheat and final results during the 2009–2010 growing season. (a) Identification results of pure winter wheat P_A with 250 m resolution. (b) Identification results of 250 m mixed pixels M_A covering winter wheat. (c) Identification results of 250 m mixed pixels M_B covering winter wheat. (d) Final winter wheat identification result with 25 m resolution.

in Fig. 9a. It can be seen that the identified pure winter wheat pixels are distributed both in a homogeneous plain, for instance in the northeast part of the study area, and in valleys with large areas of cultivated land, for instance in the western and southwestern parts. Pure pixels can only be defined at MODIS scale in these parts.

4.3. Mixed pixels M_A

For the mixed pixels of cultivated and non-cultivated land, the NDVI time series for cultivated land components are extracted based on the proposed unmixing method, before being used to separate the mixed pixels M_A from winter wheat and other vegetation, based on the same KL divergence and threshold. The results during the 2009–2010 growing season are shown in Fig. 9b. This means that the corresponding cultivated land components of the identified mixed pixels M_A cover winter wheat. That is to say, the winter wheat can be identified and extracted by combining the 25 m cultivated land data based on the spatial relationship. Usually, the mixed pixels M_A may appear on the borders between cultivated land and any other vegetation; thus, it can be seen that the mixed pixels are distributed throughout the study area.

4.4. Mixed pixels M_B

The mixed pixels M_B comprising winter wheat and other crops appear on the border of pure winter wheat P_A within the pure cultivated pixels. Using the obtained mask, winter wheat can be extracted based on temporal differences. Because the area of this mask is relatively small and lacks complicated objects, winter wheat is easily identifiable. The extracted mixed pixels M_B during the 2009–2010 growing season are shown in Fig. 9c.

In addition to winter wheat, other crops, such as cole, spring maize, leeks and garlic, appear in the study area during the same growing season according to the field investigation. However, they have distinctly different spectral and phenological characteristics from winter wheat. Therefore, they will not affect the results of the winter wheat identification.

4.5. Final results and accuracy

Combining the land use data, the final winter wheat planting area at a 25 m resolution can be obtained based on the spatial relationship, as shown in Fig. 9d. The statistics of identified winter wheat pixels, including identified MODIS pixels and the corresponding winter wheat pixels, are shown in Table 1.

The pixels P_A are pure winter wheat pixels, and the identified acreage is 63,425.00 hm^2. The cultivated land components of pixels M_A, i.e., winter wheat, are extracted based on the spatial relationship. The acreage is 70,680.00 hm^2, accounting for 47.21% of the identified MODIS pixels M_A. Winter wheat is identified based on the temporal difference in the M_B mask. The acreage is 26,945.00 hm^2, 38.11% of the

Table 1
The identified results of various pixels and their area during the 2009–2010 growing season.

Pixel type	P_A	M_A	M_B	SUM
Number of identified MODIS pixels (250 m)	10,148	23,954	11,314	45,416
Number of corresponding winter wheat pixels (25 m)	1,014,800	1,130,880	431,120	2,576,800
Winter wheat acreage (hm^2)	63,425.00	70,680.00	26,945.00	161,050.00

Table 2
Validation of winter wheat identified results.

Identification	References		UA
	Non-winter wheat	Winter wheat	
Non-winter wheat	99	11	90.00%
Winter wheat	15	375	96.15
PA	86.84%	97.15%	
OA	94.80%		

identified MODIS pixels M_B. Finally, the identified winter wheat acreage is 161,050 hm^2, the sum of the three previous results.

In the accuracy assessment of the identification result, 500 interpreted validation points are considered as "true" values and are used to validate the final result of this study. The confusion matrix is shown in Table 2. Overall accuracy is 94.80% and Kappa coefficient is 0.85. The official statistics data shows that the winter wheat planting acreage is 156,821.47 hm^2 in the study area, while the identified acreage is 161,050.00 hm^2. Relative error is only 2.70%.

5. Discussion

5.1. Separability of winter wheat

When identifying crops, there are different effects for different parameters (Comber et al., 2016; Löw et al., 2015). To illustrate this problem, we set two profile lines, shown in Fig. 4a, to compare spatial profiles for different parameters in the study area. The left profile line is Num.1 and the right is Num.2. One node is set on the profiles at every 200 m from A (C) to B (D). As a result, there are a total of 85 nodes per profile. Using the two profiles, we compared three parameters. (1) The DN value of near infrared band derived from the used TM image. It is selected since the near infrared band plays an important role in the remote sensing interpretation (Robinson et al., 2016). (2) The NDVI value at time corresponding to point D of Fig. 8. It can be seen that the greatest difference between the NDVI of winter wheat and of other vegetation is located at time corresponding to point D. (3) The last is the KL divergence for winter wheat, which is used to identify winter wheat. The spatial profile curves of these three parameters are shown in Fig. 10.

From Fig. 10, it can be seen that the winter wheat does not have any obvious spectral features in the near infrared band that are different from other vegetation. The profile's slow change indicates that it is difficult to distinguish winter wheat using the near infrared spectrum. NDVI can detect the growth status of vegetation, eliminate partial radiation errors and highlight vegetation information (Jönsson and Eklundh, 2004). At the time of D point in particular, NDVI can highlight winter wheat because it is growing vigorously while other vegetation is beginning to recover. In the NDVI profile, the value of winter wheat is higher than that of other vegetation. This is useful for distinguishing winter wheat. However, there is no clear boundary between winter wheat and other vegetation, and winter wheat's internal difference is obvious. This will cause some identification errors. The KL divergence is a measure of the difference of two probability distributions, and the smaller it is the more similar the two distributions are. Thus, it can be found that winter wheat has a homogeneous range of values and distinct boundaries from other vegetation in the spatial profile of the KL divergence. This allows the use of a threshold method to identify winter wheat. In the Num.2 profile, there are two small protrusions in the winter wheat section because the profile line crossed two non-winter wheat objects. That is, any small non-winter wheat object can affect the KL divergence value. It is therefore necessary to avoid these objects when selecting pure winter wheat samples.

5.2. Differences in various crop types

Large areas of contiguous cultivation are located in the northeastern part of the study area. Most of the remaining cultivated land is in the valley, is striped and constitutes a small area. These distribution characteristics make it possible to find pure pixels only in some areas at a MODIS scale. Winter wheat is the main wintering crop and dominant in the study area. It is relatively easy to find pure pixels, which are shown in Fig. 4a. During the winter wheat growing season, other crops such as cole, spring maize, leeks and garlic appear. However, they are mostly of small acreage and are distributed either on sloping land in mountainous areas or as intercrops. At the same time, there are also many fallow cultivated lands in the northern mountain areas of the study area.

The pure pixels of various crops can be obtained from TM images with the aid of field data. Following this, based on these pure pixels, the maximum, minimum and mean values of the KL divergence for winter wheat can be extracted, as shown in Fig. 11 where it can be seen that values for winter wheat are markedly different, with almost no overlap with other crops. This demonstrates that the KL divergence is an effective method for identifying crop types.

The proposed identification method takes full advantage of the temporal change characteristics of crops in the identification process. Because of the differences in phenological characteristics, such as planting time, growth patterns and harvest time, the method can theoretically be used for the identification of multiple crops. However, the key is to have enough planting areas for other crops and be suitable at the TM scale. If these conditions are satisfied, pure winter wheat pixels P_A and pure other crop pixels P_B are identified based on temporal features, after which the mixed pixels M_B can also be directly determined by removing P_A and P_B from the cultivated land. Subsequently, the final result will be obtained according to the flowchart that is shown in Fig. 3. This is our further research objective, which will be tested in a larger study area.

5.3. Effects of the proposed method

Compared to single data sets, multi-temporal datasets can decrease classification uncertainty for different crops (Löw et al., 2015). Based on the proposed identification method, we make full use of the time series of vegetation indices reflecting the crop growth state, and we obtain a good research result in this paper. OA and Kappa are 94.8% and 0.850, respectively. As the most commonly used classification method, the maximum likelihood method (MLC) is also utilized to extract winter wheat based only on the TM image under the same conditions. When using the same validation method, the results show that OA and Kappa are 84.6% and 0.614, respectively. We also applied random forest classification (RFC), and the result shows that OA and Kappa are 85.2% and 0.637, respectively. One of the reasons for this may be that the image acquired time is not located in the ideal temporal window. Based on Fig. 8, it can be found that the maximum difference between winter wheat and other vegetation is at point D. But the cloudless high-quality Landsat image only appeared in our study area on May 2 of this growing season. This is a disadvantage that occurs when only using spectral information. This fully demonstrates the effectiveness of combining spectral and temporal information in extraction of crop types.

However, this proposed method also has some shortcomings. For example, there is an implicit assumption in extracting mixed pixels M_A: the cultivated land component is considered to be one crop type. If the NDVI time series characteristics of this cultivated land component are consistent with winter wheat, it will be identified as winter wheat. This simultaneously proved that at the very least winter wheat dominates in this particular component. Thus, this hypothesis has little influence on the whole research result. In addition, the mixed pixel M_B is obtained by expanding the pure pixel P_A from the cultivated land. This will cause a slightly larger than actual M_B. However, it will not increase the

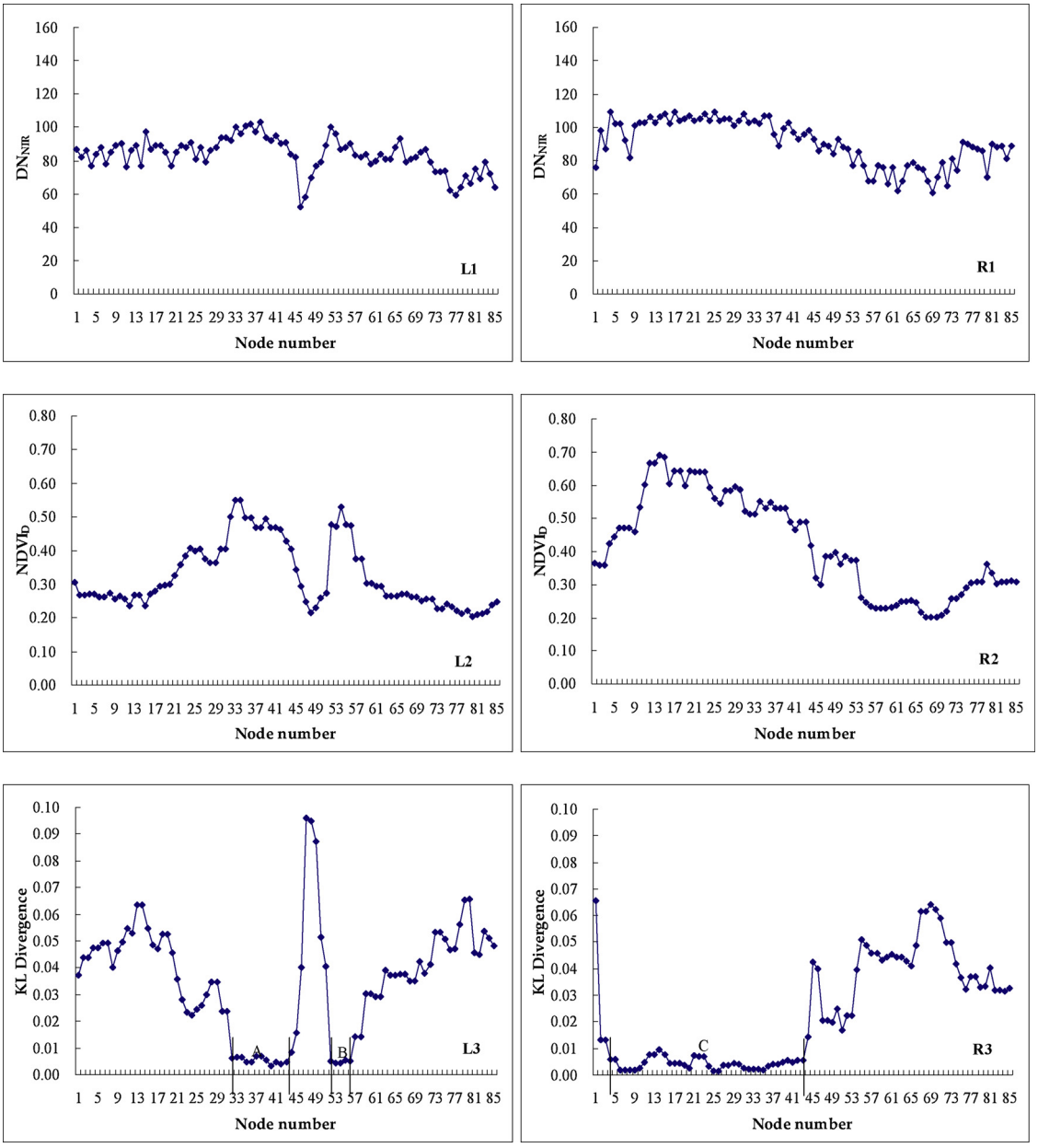

Fig. 10. Comparison of spatial profiles for different parameters. The three figures (L1–L3) on the left are generated based on the Num.1 profile line, and the three figures (R1–R3) on the right are generated based on Num.2 profile line (A, B and C are winter wheat planting areas).

identification difficulty because winter wheat dominates the study area and other crops have distinct temporal characteristics during the same growing season.

6. Conclusions

In agricultural applications of remote sensing, commonly used optical images with fine resolution possess multi-spectral and spatial resolution advantages. However, the reflectance similarity of different objects and the reflectance variability of identical objects make it difficult to further improve the classification accuracy when using only spectral properties (Yang et al., 2011). In addition, the main limiting factor is weather conditions because images of a certain point in time that are urgently needed are sometimes not obtainable, even if the satellite transits (Whitcraft et al., 2015; Ju and Roy, 2008; Roy et al., 2008). Low spatial resolution remote sensing images have an obvious temporal advantage, in that they can regularly capture the vegetation growth process. Thus, there are very significant advantages in combining low and medium spatial resolution remote sensing (Wessels et al., 2004). This study proposed a new identification method, combining these two types of images to obtain final results that present the actual crop acreage and spatial distribution at a fine scale. It also integrated the advantages of two types of research methods: temporal profile similarities based and sub-pixels mapping methods. The results proved the effectiveness of the proposed method. Another benefit is that the temporal change information can be merged in order to improve identification accuracy when ideal optical images cannot be obtained.

Through this research, we found: (1) The KL divergence of winter wheat has a clear boundary that makes it more convenient to identify winter wheat because the growth process of winter wheat is significantly different from that of other vegetation growing in the study area. During this process, the most important component is to find pure winter wheat samples and to extract the NDVI time series curve which

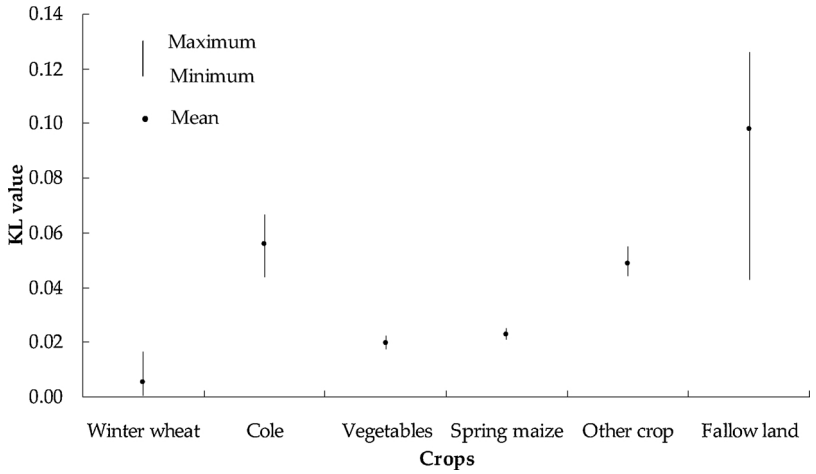

Fig. 11. KL divergence maximum, minimum and mean values for various crops during the winter wheat growing season in the study area.

is used as a reference to calculate the KL divergence. (2) Different crops have distinct temporal change characteristics. Therefore, the approaches combining temporal change information and other information deserve more attention. (3) This research provided a new perspective for the combination of low and medium spatial resolution remote sensing images. The KL divergence was not only used in identifying pure pixels but also in identifying sub-pixels, and we obtained the identification results at a fine scale.

The proposed method is mainly based on the temporal change characteristics of crops during the growing season. Therefore, it can be effectively applied in other places where the identified object has phenological characteristics that are different from those of other objects, i.e., not only for winter wheat, but also for other crops. In this study, winter wheat is dominant during this growing season and we only considered winter wheat as an identified object. Yet in actual fact, our solution has a potential to identify a variety of crop types. This will prompt us to improve the proposed pixel unmixing method. Our next goal is, therefore, to put this idea into practice. In addition, the proposed solution needs to be further optimized due to the implicit assumption that has been described above.

Acknowledgments

We acknowledge the financial support provided by the National Science and Technology Platform Construction Project (2005DKA32300), the Key Science and Technology Projects of Henan Province, China (152102110047), the Major Research Projects of the Ministry of Education (16JJD770019), the Science and Technology Development Plan Project of Henan Province, China (121100111300) Cooperation Base Open Fund of the Key Laboratory of Geospatial Technology for the middle and lower Yellow River regions and CPGIS (JOF 201602). We especially thank the anonymous reviewers for their constructive comments and insightful suggestions that greatly improved the quality of this manuscript.

References

Aguilar, C., Zinnert, J.C., Polo, M.J., Young, D.R., 2012. NDVI as an indicator for changes in water availability to woody vegetation. Ecol. Indic. 23, 290–300. https://doi.org/10.1016/j.ecolind.2012.04.008.

Amorós-López, J., Gómez-Chova, L., Alonso, L., Guanter, L., Zurita-Milla, R., Moreno, J., Camps-Valls, G., 2013. Multitemporal fusion of Landsat/TM and ENVISAT/MERIS for crop monitoring. Int. J. Appl. Earth Obs. Geoinf. 23, 132–141. https://doi.org/10.1016/j.jag.2012.12.004.

Atkinson, P.M., 1997. Mapping sub-pixel boundaries from remotely sensed images. Innovation in GIS IV. Taylor and Francis, London, UK, pp. 166–180.

Atzberger, C., Rembold, F., 2013. Mapping the spatial distribution of winter crops at sub-pixel level using AVHRR NDVI time series and neural nets. Remote Sens. 5, 1335–1354. https://doi.org/10.3390/rs5031335.

Busetto, L., Meroni, M., Colombo, R., 2008. Combining medium and coarse spatial resolution satellite data to improve the estimation of sub-pixel NDVI time series. Remote Sens. Environ. 112, 118–131. https://doi.org/10.1016/j.rse.2007.04.004.

Castillejo-González, I.L., López-Granados, F., García-Ferrer, A., Peña-Barragán, J.M., Jurado-Expósito, M., de la Orden, M.S., González-Audicana, M., 2009. Object- and pixel-based analysis for mapping crops and their agro-environmental associated measures using QuickBird imagery. Comput. Electron. Agric. 68, 207–215. https://doi.org/10.1016/j.compag.2009.06.004.

Chen, J., Jönsson, P., Tamura, M., Gu, Z., Matsushita, B., Eklundh, L., 2004. A simple method for reconstructing a high-quality NDVI time-series data set based on the Savitzky-Golay filter. Remote Sens. Environ. 91, 332–344. https://doi.org/10.1016/j.rse.2004.03.014.

Chmielewski, F.M., Muller, A., Bruns, E., 2004. Climate changes and trends in phenology of fruit trees and field crops in Germany, 1961–2000. Agric. For. Meteorol. 121, 69–78. https://doi.org/10.1016/S0168-1923(03)00161-8.

Comber, A.J., Harris, P., Tsutsumida, N., 2016. Improving land cover classification using input variables derived from a geographically weighted principal components analysis. ISPRS J. Photogramm. Remote Sens. 119, 347–360. https://doi.org/10.1016/j.isprsjprs.2016.06.014.

Conese, C., Maselli, F., 1991. Use of multitemporal information to improve classification performance of TM scenes in complex terrain. ISPRS J. Photogramm. Remote Sens. 46, 187–197. https://doi.org/10.1016/0924-2716(91)90052-W.

Estel, S., Kuemmerle, T., Alcantara, C., Levers, C., Prishchepov, A., Hostert, P., 2015. Mapping farmland abandonment and recultivation across Europe using MODIS NDVI time series. Remote Sens. Environ. 163, 312–325. https://doi.org/10.1016/j.rse.2015.03.028.

Everitt, J.H., Yang, C.H., Summy, K., Nachtrieb, J.G., 2013. Using hyperspectral reflectance data to assess biocontrol damage of giant salvinia. Geocarto Int. 28, 502–516. https://doi.org/10.1080/10106049.2012.724454.

FAOSTAT, 2014. Production domain. Crops. FAO.

Franch, B., Vermote, E.F., Becker-Reshef, I., Claverie, M., Huang, J., Zhang, J., Justice, C., Sobrino, J.A., 2015. Improving the timeliness of winter wheat production forecast in the United States of America, Ukraine and China using MODIS data and NCAR growing degree day information. Remote Sens. Environ. 161, 131–148. https://doi.org/10.1016/j.rse.2015.02.014.

Gandhi, G.M., Parthiban, S., Thummalu, N., Christy, A., 2015. NDVI: vegetation change detection using remote sensing and GIS—a case study of Vellore District. Procedia Comput. Sci. 57, 1199–1210. https://doi.org/10.1016/j.procs.2015.07.415.

Gao, F., Anderson, M.C., Zhang, X., Yang, Z., Alfieri, J.G., Kustas, W.P., Mueller, R., Johnson, D.M., Prueger, J.H., 2017. Toward mapping crop progress at field scales through fusion of Landsat and MODIS imagery. Remote Sens. Environ. 188, 9–25. https://doi.org/10.1016/j.rse.2016.11.004.

Ghiyamat, A., Shafri, H.Z.M., Mahdiraji, G.A., Shariff, A.R.M., Mansor, S., 2013. Hyperspectral discrimination of tree species with different classifications using single- and multiple-endmember. Int. J. Appl. Earth Obs. Geoinf. 23, 177–191. https://doi.org/10.1016/j.jag.2013.01.004.

Gumma, M.K., Mohanty, S., Nelson, A., Arnel, R., Mohammed, I.A., Das, S.R., 2015. Remote sensing based change analysis of rice environments in Odisha, India. J. Environ. Manage. 148, 31–41. https://doi.org/10.1016/j.jenvman.2013.11.039.

Hao, P.Y., Zhan, Y.L., Wang, L., Niu, Z., Shakir, M., 2015. Feature selection of time series MODIS data for early crop classification using random forest: a case study in Kansas, USA. Remote Sens. 7, 5347–5369. https://doi.org/10.3390/rs70505347.

He, L., Asseng, S., Zhao, G., Wu, D., Yang, X., Zhuang, W., Jin, N., Yu, Q., 2015. Impacts of recent climate warming, cultivar changes, and crop management on winter wheat phenology across the Loess Plateau of China. Agric. For. Meteorol. 200, 135–143. https://doi.org/10.1016/j.agrformet.2014.09.011.

Homolova, L., Maenovsky, Z., Clevers, J., Garcia-Santos, G., Schaeprnan, M.E., 2013. Review of optical-based remote sensing for plant trait mapping. Ecol. Complex. 15, 1–16. https://doi.org/10.1016/j.ecocom.2013.06.003.

Huang, X., Schneider, A., Friedl, M.A., 2016. Mapping sub-pixel urban expansion in China

using MODIS and DMSP/OLS nighttime lights. Remote Sens. Environ. 175, 92–108. https://doi.org/10.1016/j.rse.2015.12.042.
Jin, X., Kumar, L., Li, Z., Xu, X., Yang, G., Wang, J., 2016. Estimation of winter wheat biomass and yield by combining the AquaCrop model and field hyperspectral data. Remote Sens. 8, 972. https://doi.org/10.3390/rs8120972.
Jönsson, P., Eklundh, L., 2004. TIMESAT—a program for analyzing time-series of satellite sensor data. Comput. Geosci. 30, 833–845. https://doi.org/10.1016/j.cageo.2004.05.006.
Ju, J., Roy, D.P., 2008. The availability of cloud-free Landsat ETM+ data over the conterminous United Sates and globally. Remote Sens. Environ. 112, 1196–1211. https://doi.org/10.1016/j.rse.2007.08.011.
Kasetkasem, T., Arora, M.K., Varshney, P.K., 2005. Super-resolution land cover mapping using a Markov random field based approach. Remote Sens. Environ. 96, 302–314. https://doi.org/10.1016/j.rse.2005.02.006.
Kullback, S., Leibler, R.A., 1951. On information and sufficiency. Ann. Math. Stat. 22, 79–86. https://doi.org/10.1214/aoms/1177729694.
Landmann, T., Piiroinen, R., Makori, D.M., Abdel-Rahman, E.M., Makau, S., Pellikka, P., Raina, S.K., 2015. Application of hyperspectral remote sensing for flower mapping in African savannas. Remote Sens. Environ. 166, 50–60. https://doi.org/10.1016/j.rse.2015.06.006.
Langley, S.K., Cheshire, H.M., Humes, K.S., 2001. A comparison of single date and multitemporal satellite image classification in a semi-arid grassland. J. Arid Environ. 49, 401–411. https://doi.org/10.1006/jare.2000.0771.
Lhermitte, S., Verbesselt, J., Verstraeten, W.W., Coppin, P., 2011. A comparison of time series similarity measures for classification and change detection of ecosystem dynamics. Remote Sens. Environ. 115, 3129–3152. https://doi.org/10.1016/j.rse.2011.06.020.
Liaghat, S., Balasundram, S.K., 2010. A review: the role of remote sensing in precision agriculture. Am. J. Agric. Biol. Sci. 5, 553–564. https://doi.org/10.3844/ajabssp.2010.50.55.
Li, H., Chen, Z., Liu, G., Jiang, Z., Huang, C., 2017. Improving winter wheat yield estimation from the CERES-wheat model to assimilate leaf area index with different assimilation methods and spatio-temporal scales. Remote Sens. 9, 190. https://doi.org/10.3390/rs9030190.
Yang, Z., Wu, W., Di, L., Üstündağ, B., 2017. Remote sensing for agricultural applications. J. Integr. Agric. 16, 239–241. https://doi.org/10.1016/S2095-3119(16)61549-6.
Li, S., Xiao, J., Ni, P., Zhang, J., Wang, H., Wang, J., 2014. Monitoring paddy rice phenology using time series MODIS data over Jiangxi Province. China. Int. J. Agric. Biol. Eng. 7, 28–36. https://doi.org/10.3965/j.ijabe.20140706.005.
Lobell, D.B., Asner, G.P., 2004. Cropland distribution from temporal unmixing of MODIS data. Remote Sens. Environ. 93, 412–422. https://doi.org/10.1016/j.rse.2004.08.002.
Lobell, D.B., Thau, D., Seifert, C., Engle, E., Little, B., 2015. A scalable satellite-based crop yield mapper. Remote Sens. Environ. 164, 324–333. https://doi.org/10.1016/j.rse.2015.04.021.
Löw, F., Knöfel, P., Conrad, C., 2015. Analysis of uncertainty in multi-temporal object-based classification. ISPRS J. Photogramm. Remote Sens. 105, 91–106. https://doi.org/10.1016/j.isprsjprs.2015.03.004.
Martínez-Casasnovas, J.A., Martín-Montero, A., Casterad, M.A., 2005. Mapping multi-year cropping patterns in small irrigation districts from time–series analysis of Landsat TM images. Eur. J. Agron. 23, 159–169. https://doi.org/10.1016/j.eja.2004.11.004.
Mertens, K.C., Verbeke, L.P.C., Ducheyne, E.I., De Wulf, R.R., 2003. Using genetic algorithms in sub-pixel mapping. Int. J. Remote Sens. 24, 4241–4247. https://doi.org/10.1080/0143116031000595073.
Mertens, K.C., Verbeke, L.P.C., Westra, T., De Wulf, R.R., 2004. Sub-pixel mapping and sub-pixel sharpening using neural network predicted wavelet coefficients. Remote Sens. Environ. 91, 225–236. https://doi.org/10.1016/j.rse.2004.03.003.
NSPRC(National Standards of People's Republic of China (GB/T 17296-2009)), 2009. Classification and Codes for Chinese Soil. Standards Press of China, Beijing, China.
Olszewski, D., 2012. A probabilistic approach to fraud detection in telecommunications. Knowl.—Based Syst. 26, 246–258. https://doi.org/10.1016/j.knosys.2011.08.018.
Pan, Y., Li, L., Zhang, J., Liang, S., Zhu, X., Sulla-Menashe, D., 2012. Winter wheat area estimation from MODIS-EVI time series data using the Crop Proportion Phenology Index. Remote Sens. Environ. 119, 234–242. https://doi.org/10.1016/j.rse.2011.10.011.
Pax-Lenney, M., Woodcock, C.E., Macomber, S.A., Gopal, S., Song, C., 2001. Forest mapping with a generalized classifier and Landsat TM data. Remote Sens. Environ. 77, 241–250. https://doi.org/10.1016/S0034-4257(01)00208-5.
Potapov, P., Hansen, M.C., Stehman, S.V., Loveland, T.R., Pittman, K., 2008. Combining MODIS and Landsat imagery to estimate and map boreal forest cover loss. Remote Sens. Environ. 112, 3708–3719. https://doi.org/10.1016/j.rse.2008.05.006.
Qin, Y., Xiao, X., Dong, J., Zhou, Y., Zhu, Z., Zhang, G., Du, G., Jin, C., Kou, W., Wang, J., Li, X., 2015. Mapping paddy rice planting area in cold temperate climate region through analysis of time series Landsat 8 (OLI), Landsat 7 (ETM+) and MODIS imagery. ISPRS J. Photogramm. Remote Sens. 105, 220–233. https://doi.org/10.1016/j.isprsjprs.2015.04.008.
Qiu, B., Luo, Y., Tang, Z., Chen, C., Lu, D., Huang, H., Chen, Y., Chen, N., Xu, W., 2017. Winter wheat mapping combining variations before and after estimated heading dates. ISPRS J. Photogramm. Remote Sens. 123, 35–46. https://doi.org/10.1016/j.isprsjprs.2016.09.016.
Ren, J., Chen, Z., Zhou, Q., Tang, H., 2008. Regional yield estimation for winter wheat with MODIS-NDVI data in Shandong, China. Int. J. Appl. Earth Obs. Geoinf. 10, 403–413. https://doi.org/10.1016/j.jag.2007.11.003.
Robinson, T.P., Wardell-Johnson, G.W., Pracilio, G., Brown, C., Corner, R., van Klinken, R.D., 2016. Testing the discrimination and detection limits of WorldView-2 imagery on a challenging invasive plant target. Int. J. Appl. Earth Obs. Geoinf. 44, 23–30. https://doi.org/10.1016/j.jag.2015.07.004.
Roy, D.P., Ju, J., Lewis, P., Schaaf, C., Gao, F., Hansen, M., Lindquist, E., 2008. Multi-temporal MODIS-Landsat data fusion for relative radiometric normalization, gap filling, and prediction of Landsat data. Remote Sens. Environ. 112, 3112–3130. https://doi.org/10.1016/j.rse.2008.03.009.
Sakamoto, T., Yokozawa, M., Toritani, H., Shibayama, M., Ishitsuka, N., Ohno, H., 2005. A crop phenology detection method using time-series MODIS data. Remote Sens. Environ. 96, 366–374. https://doi.org/10.1016/j.rse.2005.03.008.
Siachalou, S., Mallinis, G., Tsakiri-Strati, M., 2015. A hidden Markov models approach for crop classification: linking crop phenology to time series of multi-sensor remote sensing data. Remote Sens. 7, 3633–3650. https://doi.org/10.3390/rs70403633.
Sun, H., Xu, A., Lin, H., Zhang, L., Mei, Y., 2012. Winter wheat mapping using temporal signatures of MODIS vegetation index data. Int. J. Remote Sens. 33, 5026–5042. https://doi.org/10.1080/01431161.2012.657366.
Tao, J., Wu, W., Zhou, Y., Wang, Y., Yan, J., 2017. Mapping winter wheat using phenological feature of peak before winter on the North China Plain based on time-series MODIS data. J. Integr. Agr. 16, 348–359. https://doi.org/10.1016/S2095-3119(15)61304-1.
Tatem, A.J., Lewis, H.G., Atkinson, P.M., Nixon, M.S., 2002. Super-resolution land cover pattern prediction using a Hopfield neural network. Remote Sens. Environ. 79, 1–14. https://doi.org/10.1016/S0034-4257(01)00229-2.
Tatem, A.J., Lewis, H.G., Atkinson, P.M., Nixon, M.S., 2001. Superresolution target identification from remotely sensed images using a Hopfield neural network. IEEE Trans. Geosci. Remote Sens. 39, 781–796. https://doi.org/10.1109/36.917895.
Thornton, M.W., Atkinson, P.M., Holland, D.A., 2006. Sub-pixel mapping of rural land cover objects from fine spatial resolution satellite sensor imagery using super-resolution pixel-swapping. Int. J. Remote Sens. 27, 473–491. https://doi.org/10.1080/01431160500207088.
Upadhyay, P., Ghosh, S.K., Kumar, A., 2015. Temporal MODIS data for identification of wheat crop using noise clustering soft classification approach. Geocarto Int. 31, 278–295. https://doi.org/10.1080/10106049.2015.1047415.
van Lier, O.R., Fournier, R.A., Bradley, R.L., Thiffault, N., 2009. A multi-resolution satellite imagery approach for large area mapping of ericaceous shrubs in Northern Quebec, Canada. Int. J. Appl. Earth Obs. Geoinf. 11, 334–343. https://doi.org/10.1016/j.jag.2009.05.003.
Verhoeye, J., De Wulf, R., 2002. Land cover mapping at sub-pixel scales using linear optimization techniques. Remote Sens. Environ. 79, 96–104. https://doi.org/10.1016/S0034-4257(01)00242-5.
Vorobiova, N., Chernov, A., 2017. Curve fitting of MODIS NDVI time series in the task of early crops identification by satellite images. Procedia Eng. 201, 184–195. https://doi.org/10.1016/j.proeng.2017.09.596.
Waldhoff, G., Lussem, U., Bareth, G., 2017. Multi-Data Approach for remote sensing-based regional crop rotation mapping: A case study for the Rur catchment, Germany. Int. J. Appl. Earth Obs. Geoinf. 61, 55–69. https://doi.org/10.1016/j.jag.2017.04.009.
Waldner, F., Lambert, M.J., Li, W.J., Weiss, M., Demarez, V., Morin, D., Marais-Sicre, C., Hagolle, O., Baret, F., Defourny, P., 2015. Land cover and crop type classification along the season based on biophysical variables retrieved from multi-sensor high-resolution time series. Remote Sens. 7, 10400–10424. https://doi.org/10.3390/rs70810400.
Wang, C., Fan, Q., Li, Q., SooHoo, W.M., Lu, L., 2017. Energy crop mapping with enhanced TM/MODIS time series in the BCAP agricultural lands. ISPRS J. Photogramm. Remote Sens. 124, 133–143. https://doi.org/10.1016/j.isprsjprs.2016.12.002.
Wang, L., Gong, P., Ying, Q., Yang, Z., Cheng, X., Ran, Q., 2010. Settlement extraction in the North China Plain using Landsat and Beijing-1 multispectral data with an improved watershed segmentation algorithm. Int. J. Remote Sens. 31, 1411–1426. https://doi.org/10.1080/01431160903475332.
Wang, Q., Atkinson, P.M., 2017. The effect of the point spread function on sub-pixel mapping. Remote Sens. Environ. 193, 127–137. https://doi.org/10.1016/j.rse.2017.03.002.
Wardlow, B.D., Egbert, S.L., 2010. A comparison of MODIS 250-m EVI and NDVI data for crop mapping: a case study for southwest Kansas. Int. J. Remote Sens. 31, 805–830. https://doi.org/10.1080/01431160902897858.
Wessels, K.J., De Fries, R.S., Dempewolf, J., Anderson, L.O., Hansen, A.J., Powell, S.L., Moran, E.F., 2004. Mapping regional land cover with MODIS data for biological conservation: examples from the Greater Yellowstone Ecosystem, USA and Pará State, Brazil. Remote Sens. Environ. 92, 67–83. https://doi.org/10.1016/j.rse.2004.05.002.
Wetherley, E.B., Roberts, D.A., McFadden, J.P., 2017. Mapping spectrally similar urban materials at sub-pixel scales. Remote Sens. Environ. 195, 170–183. https://doi.org/10.1016/j.rse.2017.04.013.
Whitcraft, A.K., Vermote, E.F., Becker-Reshef, I., Justice, C.O., 2015. Cloud cover throughout the agricultural growing season: impacts on passive optical earth observations. Remote Sens. Environ. 156, 438–447. https://doi.org/10.1016/j.rse.2014.10.009.
Wu, B., Li, Q., 2012. Crop planting and type proportion method for crop acreage estimation of complex agricultural landscapes. Int. J. Appl. Earth Obs. Geoinf. 16, 101–112. https://doi.org/10.1016/j.jag.2011.12.006.
Wu, M., Huang, W., Niu, Z., Wang, Y., Wang, C., Li, W., Hao, P., Yu, B., 2017. Fine crop mapping by combining high spectral and high spatial resolution remote sensing data in complex heterogeneous areas. Comput. Electron. Agric. 139, 1–9. https://doi.org/10.1016/j.compag.2017.05.003.
Wu, M., Wu, C., Huang, W., Niu, Z., Wang, C., Li, W., Hao, P., 2016a. An improved high spatial and temporal data fusion approach for combining Landsat and MODIS data to generate daily synthetic Landsat imagery. Inform. Fusion. 31, 14–25. https://doi.org/10.1016/j.inffus.2015.12.005.

Wu, W., Yang, X., Liu, K., Liu, Y., Yan, B., Hua, H., 2016b. A new framework for remote sensing image super-resolution: sparse representation-based method by processing dictionaries with multi-type features. J. Syst. Architect. 64, 63–75. https://doi.org/10.1016/j.sysarc.2015.11.005.

Wu, M., Zhang, X., Huang, W., Niu, Z., Wang, C., Li, W., Hao, P., 2015. Reconstruction of Daily 30 m Data from HJ CCD, GF-1 WFV, Landsat, and MODIS data for crop monitoring. Remote Sens. 7, 16293–16314. https://doi.org/10.3390/rs71215826.

Xu, J., Denman, S., Fookes, C., Sridharan, S., 2016. Detecting rare events using Kullback–Leibler divergence: a weakly supervised approach. Expert Syst. Appl. 54, 13–28. https://doi.org/10.1016/j.eswa.2016.01.035.

Yang, C., Everitt, J.H., Murden, D., 2011. Evaluating high resolution SPOT 5 satellite imagery for crop identification. Comput. Electron. Agric. 75, 347–354. https://doi.org/10.1016/j.compag.2010.12.012.

Yusoff, N.M., Muharam, F.M., 2015. The use of multi-temporal landsat imageries in detecting seasonal crop abandonment. Remote Sens. 7, 11974–11991. https://doi.org/10.3390/rs70911974.

Zhang, X., Qin, Y., Qin, F., 2013. Remote sensing estimation of planting area for winter wheat by integrating seasonal rhythms and spectral characteristics. Trans. CSAE 29, 154–163. https://doi.org/10.3969/j.issn.1002-6819.2013.08.018. (in Chinese with English abstract).

Zhang, X., 2009. Extraction and Application of Valid Vegetation Cover for Water Erosion Risk Assessment. PhD Dissertation, Institute of Remote Sensing Applications Chinese Academy of Sciences, Beijing.

Zheng, B., Campbell, J.B., de Beurs, K.M., 2012. Remote sensing of crop residue cover using multi-temporal Landsat imagery. Remote Sens. Environ. 117, 177–183. https://doi.org/10.1016/j.rse.2011.09.016.

Zhong, Y., Wu, Y., Zhang, L., Xu, X., 2014. Adaptive MAP sub-pixel mapping model based on regularization curve for multiple shifted hyperspectral imagery. ISPRS J. Photogramm. Remote Sens. 96, 134–148. https://doi.org/10.1016/j.isprsjprs.2014.06.019.

Zhou, T., Pan, J., Zhang, P., Wei, S., Han, T., 2017. Mapping winter wheat with multi-temporal SAR and optical images in an urban agricultural region. Sensors 17, 1210. https://doi.org/10.3390/s17061210.

Zhou, Y., Qiu, F., 2015. Fusion of high spatial resolution world view-2 imagery and LiDAR pseudo-waveform for object-based image analysis. ISPRS J. Photogramm. Remote Sens. 101, 221–232. https://doi.org/10.1016/j.isprsjprs.2014.12.013.

Zhu, X., Helmer, E.H., Gao, F., Liu, D., Chen, J., Aefsky, M.A., 2016. A flexible spatio-temporal method for fusing satellite images with different resolutions. Remote Sens. Environ. 172, 165–177. https://doi.org/10.1016/j.rse.2015.11.016.